Cell Death &
Differentiation

ARTICLE

Stepwise activation of the pro-apoptotic protein Bid at mitochondrial membranes

Chien-Lun Hung [1] · Hsin-Ho Chang[1] · Su Wei Lee[1] · Yun-Wei Chiang [1]

Abstract

Caspase-8-cleaved Bid (cBid) associates with mitochondria and promotes the activation of BAX, leading to mitochondria outer membrane permeabilization (MOMP) and apoptosis. However, current structural models of cBid are largely based on studies using membrane vesicles and detergent micelles. Here we employ spin-label ESR and site-directed PEGylation methods to identify conformations of cBid at real mitochondrial membranes, revealing stepwise mechanisms in the activation process. Upon the binding of cBid to mitochondria, its structure is reorganized to expose the BH3 domain while leaving the structural integrity only slightly altered. The mitochondria-bound cBid is in association with Mtch2 and it remains in the primed state until interacting with BAX. The interaction subsequently triggers the fragmentation of cBid, causes large conformational changes, and promotes BAX-mediated MOMP. Our results reveal structural differences of cBid between mitochondria and other lipid-like environments and, moreover, highlight the role of the membrane binding in modifying cBid structure and assisting the inactive-to-active transition in function.

Introduction

The BCL-2 family of proteins govern critical pathways to apoptosis by regulating mitochondrial outer membrane permeabilization (MOMP) [1, 2]. The protein family can be divided into anti- and pro-apoptotic classes according to their function and the BCL-2 homology (BH) motifs. The class of pro-apoptotic proteins can be further categorized into the multi-BH motif proteins (such as BAX and BAK) and the BH3-only proteins (such as Bim, PUMA, Bad, and Bid). The BH3-only proteins use the BH3 domain to engage and neutralize the anti-apoptotic members and probably also to promote regulated cell death by activating the critical effectors BAX and BAK, which causes MOMP and cell death. Among the BCL-2 family, Bid is the only member

that bridges the crosstalk between extrinsic and intrinsic pathways of apoptosis [3–5]. Due to the crucial role of BH3-only proteins in apoptosis, it is not surprising that much effort has been made to develop BH3-mimetic drugs as novel anti-cancer agents [6, 7].

Unlike other BH3-only proteins that are intrinsically unstructured [8], Bid has a defined structure similar to many multi-BH members [9–11]. Under apoptotic stress, cytosolic Bid is post-translationally cleaved at site D59 (Fig. 1a) by caspase-8 to produce cleaved Bid (cBid) comprising two domains, p7 and truncated Bid (tBid, also known as p15), but the overall structure of Bid is preserved after the cleavage (Supplementary Fig. 1a) [9]. Previous in vivo studies reported that only when associating with mitochondrial membranes can cBid become active [12–14] to initiate the BAX/BAK-mediated MOMP [15–18]. Structure-based evidence supported that Bid adopts an extended conformation in lipid-like environments and the conformation is critical for association with other pro-apoptotic proteins [19, 20]. Using fluorescence technique, Gahl et al. reported the intermolecular contacts between cBid and BAX at the onset of apoptosis and proposed the formation of tBid/BAX networked oligomers in live cells [19]. Recently, Lan et al. [21] provided a more specific description that the canonical and trigger grooves (TGs) [22, 23] of BAX are involved in the engagements with cBid during BAX-mediated MOMP.

Edited by: A Degterev

✉ Yun-Wei Chiang
ywchiang@gapp.nthu.edu.tw

[1] Department of Chemistry, National Tsing Hua University, Hsinchu, Taiwan
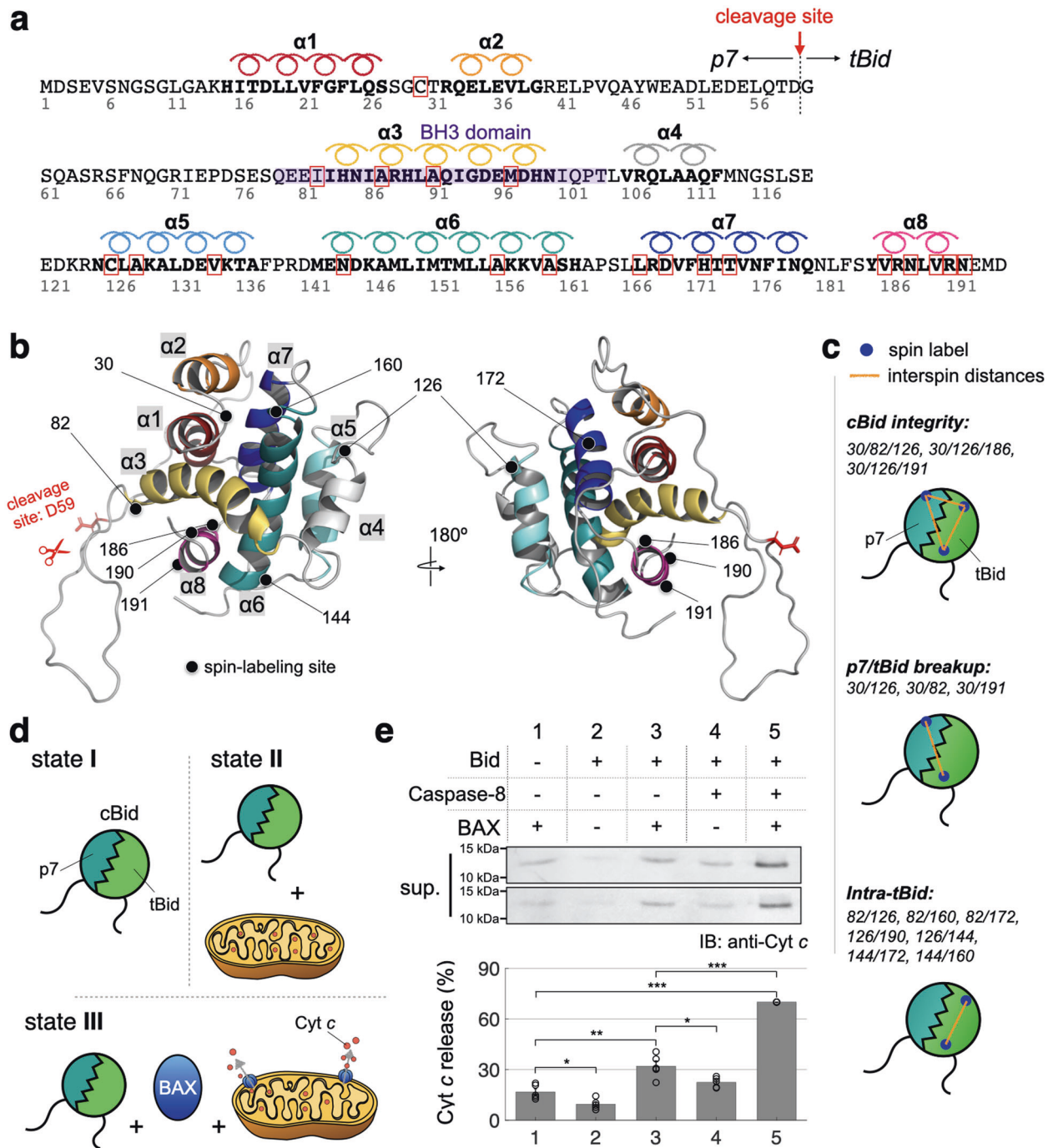
Fig. 1 Bid structure and study strategy. a Sequence of mouse Bid protein. D59 is the caspase-8 cleavage site. Red boxes indicate the residues mutated to cysteine for spin-labeling and PEGylation studies. The BH3 domain is highlighted in purple color. **b** Cartoon models displaying full-length Bid structure (PDB: 1DDB; see also Supplementary Fig. 1a). Helices are colored according to (**a**). **c** Cartoons illustrating the spin-labeling strategy of the present study. Spin-labeling sites can be categorized into three groups as indicated. **d** This study focuses on identifying the conformations of cBid in the three states indicated. **e** Assays for cytochrome *c* release from isolated mouse mitochondria. Concentrations of cBid and BAX were 20 and 100 nM, respectively. After an incubation for 30 min at 37 °C, cytochrome *c* release was detected by IB analysis of the supernatants. Error bars represent the mean ± SE from five independent experiments. (See also Supplementary Figs. 1–3.).

Although Bid activation has been extensively studied, the current structural models of Bid are established primarily based on the results of model membranes. The conformational changes in cBid during the association with real mitochondrial membranes have not been sufficiently characterized. Without the use of real mitochondria, the

possible contributions of other factors that affect the regulation of Bid could be overlooked.

The present study aims to investigate the conformational changes of cBid during the process of cBid-induced BAX oligomerization and MOMP using techniques including spin-label electron spin resonance (ESR) and PEGylation-based gel shift assay. The double electron-electron resonance (DEER) ESR technique has recently been demonstrated as a powerful tool for determining protein structure and topology in a complex membrane environment [24–28]. The DEER data provide interspin distance distributions in the range of 1.5–8 nm and the distance constraints (from the following study strategy) that can be used to determine assembly and individual structures of protein subunits. We thus perform DEER to identify the conformational changes in cBid and also explore the interactions of Bid with the mitochondrial carrier homolog 2 (Mtch2), a key protein known to play a role in facilitating the recruitment of tBid to mitochondria [29–31].

Various single-/double-/triple-cysteine variants of Bid are prepared (Fig. 1b) for spin-label ESR as well as PEGylation studies. Triply spin-labeled samples (Fig. 1c) are used to study the structural integrity of cBid during the cBid-induced BAX activation. Doubly spin-labeled cBid samples can be further divided into two groups: p7/tBid-breakup and intra-tBid groups (Fig. 1c); samples of the former allow one to explore when the breakup of cBid (i.e., p7/tBid) occur, and samples of the latter can be used to identify the conformational changes in the tBid fragment. As the cBid-induced BAX activation occurs primarily in mitochondria, this study focuses on investigating the conformations of cBid and categorizes them into three states (Fig. 1d): cBid in solution (state **I**), mitochondria-associated cBid (state **II**), and mitochondria/BAX-associated cBid (state **III**). States **II** and **III** correspond to samples in the pellet fraction of a given incubation (see Methods). The incubation of cBid with BAX in the absence of mitochondria is not studied as BAX remains inactive and monomeric in such a lipid-free incubation (Supplementary Fig. 1b). Moreover, we perform site-directed PEGylation-based assays [18, 21, 32–34] to reveal the membrane association profiles of individual helices of cBid. New insights into the details of cBid-induced BAX activation at real mitochondrial membranes are thus revealed in this study.

Results

This study categorizes the conformations of cBid in the event of cBid-induced BAX activation into three states (Fig. 1d). To demonstrate the biological significance of the categories, we performed assays for cytochrome c release from isolated mouse liver mitochondria. Cleaved Bid (cBid)

was obtained by incubating Bid with caspase-8. Lanes 4 and 5 (Fig. 1e) correspond to states **II** and **III**, respectively. The results (Fig. 1e) show that a relatively large amount of cytochrome c was released from mitochondria only when cBid was incubated with wild-type BAX (wt). (Supplementary Fig. 2 shows more supporting results performed with mitochondria isolated from the $BAX^{-/-}BAK^{-/-}$ DKO HCT116 cells. Supplementary Fig. 3 presents more control experiments showing both the supernatant and pellet fractions of mitochondria.)

Structural integrity of cBid is altered upon the association with mitochondria

To investigate the conformations of cBid, we performed DEER measurements (Fig. 2a) on the triple-labeled cBid samples, which provide information of cBid integrity, and the double-labeled cBid samples belonging to the p7/tBid-breakup group. Spin-labeled cBid 144/160 is regarded as a control as the two spin-labeled sites are within the same helix α6 and the helical conformation is expected to change little between the states. The time-domain traces of DEER measurements (Fig. 2a) showed that except for the control 144/160, the amplitude of modulation depth (denoted by V_m in Fig. 2a) for state **I** is clearly greater than those for state **III**. Careful analysis of the modulation depths can yield information on the number of spins per cluster (<N> as shown in Fig. 2b; details given in Methods) reporting an average of interacting spins per objects (or per sphere of ~6 nm radius in the ensemble) [35, 36]. <N> values in state **I** are well consistent with our expectation: close to 2 and 3 for double- and triple-labeled cBid, respectively. In state **II**, <N> values were slightly affected due to the membrane associations of cBid, which complicate the DEER signals, but they remained close to those of state **I**, supporting that cBid in state **II** retains its overall integrity and its subunits do not collapse. In state **III**, we observed a drastic decrease in <N>, indicating the breakdown of the integrity and the separation of cBid into the p7 and tBid fragments. (Supplementary Fig. 4 shows more results confirming that the breakup of p7/tBid occurs in **III**.) A cartoon illustration is provided (Fig. 2c) to show how V_m is related to the average of interacting spins per objects (<N>) calculated using the equations given in Methods.

The corresponding interspin distance distributions (Fig. 2d), extracted from the time-domain DEER data (Fig. 2a) using Tikhonov-based methods [37–39], revealed molecular details of the cBid conformations. All of the distance distributions obtained for state **I** are consistent with the predictions simulated from the NMR-based structure of Bid (PDB:1DDB [40]; see also Supplementary Fig. 1) using the MtsslWizard program [41]. There are some small but marked differences when comparing the distance distributions
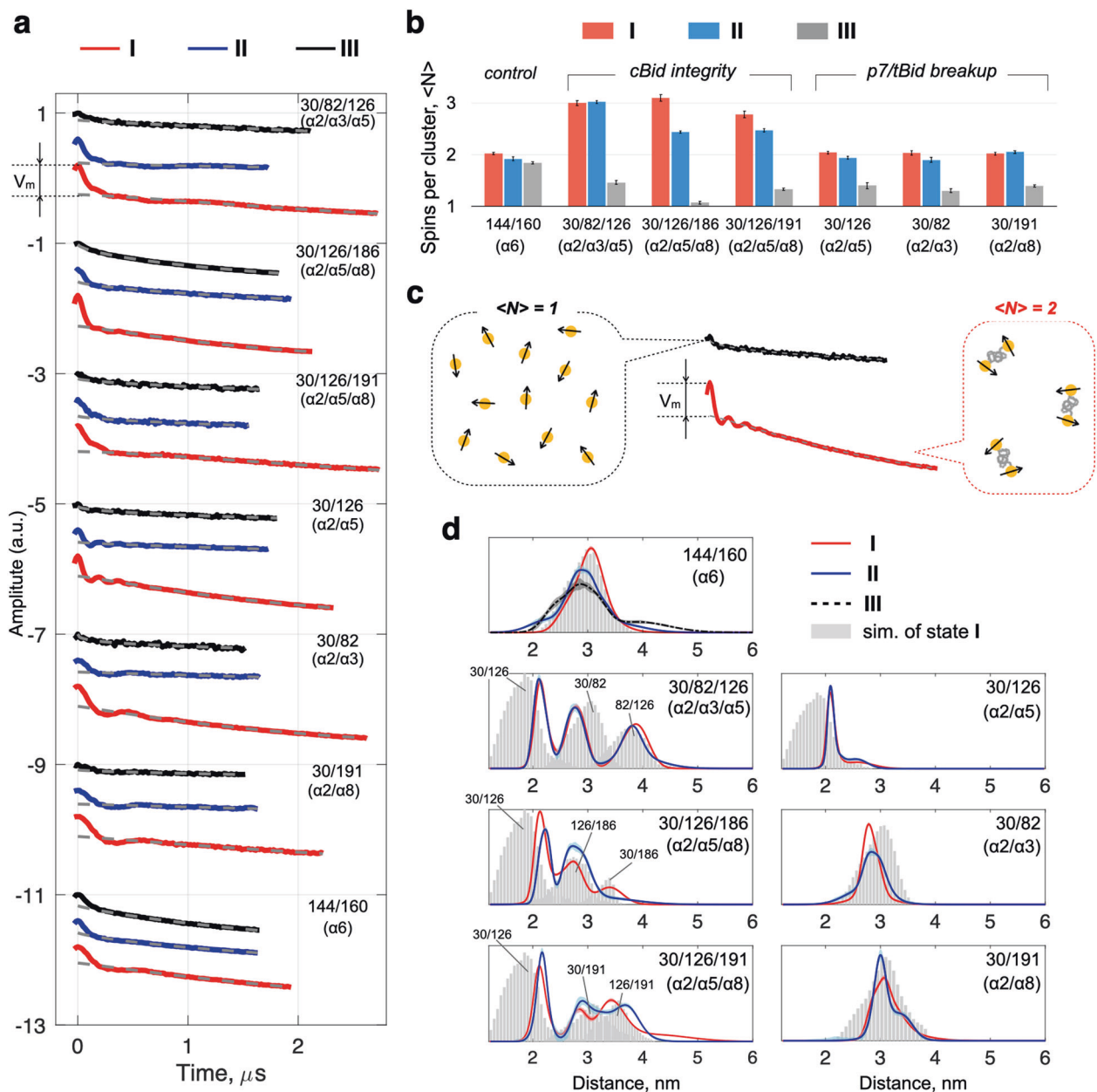
Fig. 2 DEER data of cBid. a Experimental time-domain DEER data of spin-labeled cBid. Fits to the DEER background signals are shown in gray (as detailed in Methods). As indicated, the modulation depth V_m can be directly obtained from the DEER data. **b** V_m values can be used to calculate the number of spins per cluster, <N>. 144/160 is a control demonstrating that <N> remains close to 2 in the three states. Error estimates were obtained from the data analysis using the DeerAnalysis software package. **c** Cartoon to illustrate how V_m is related to <N>. **d** Distance distributions extracted from the DEER data. Predictions simulated from the solution structure of Bid are shown in gray histograms, consistent with **I**. Conformational integrities of cBid in **I** and **II** are only slightly different. Shaded bands are estimates of uncertainty in the DEER distance distributions. See also Supplementary Table 1.

between states **I** and **II** (i.e., red versus blue lines in Fig. 2d). These differences support that cBid adopts somewhat different conformations upon the transition from state **I** to the membrane-associated state **II**. However, the structural integrity is only slightly altered as the distance peaks of the triple-labeled samples remain distinguishable in both **I** and **II**. (More details about the induced structural changes in state **II** will be discussed later.) In state **III**, except for the 144/160

result (a control), the modulation depths were too weak to allow a reliable recovery of distance distributions from the DEER data (Supplementary Fig. 5). The DEER data of state **III** were dominated by an exponential decay, indicating an ensemble of broadly and homogeneously distributed spins (see also black line in Fig. 2c). The broad distribution of spins can be attributed to partial unfolding and increased flexibility in state **III** after the interaction with BAX at mitochondria.
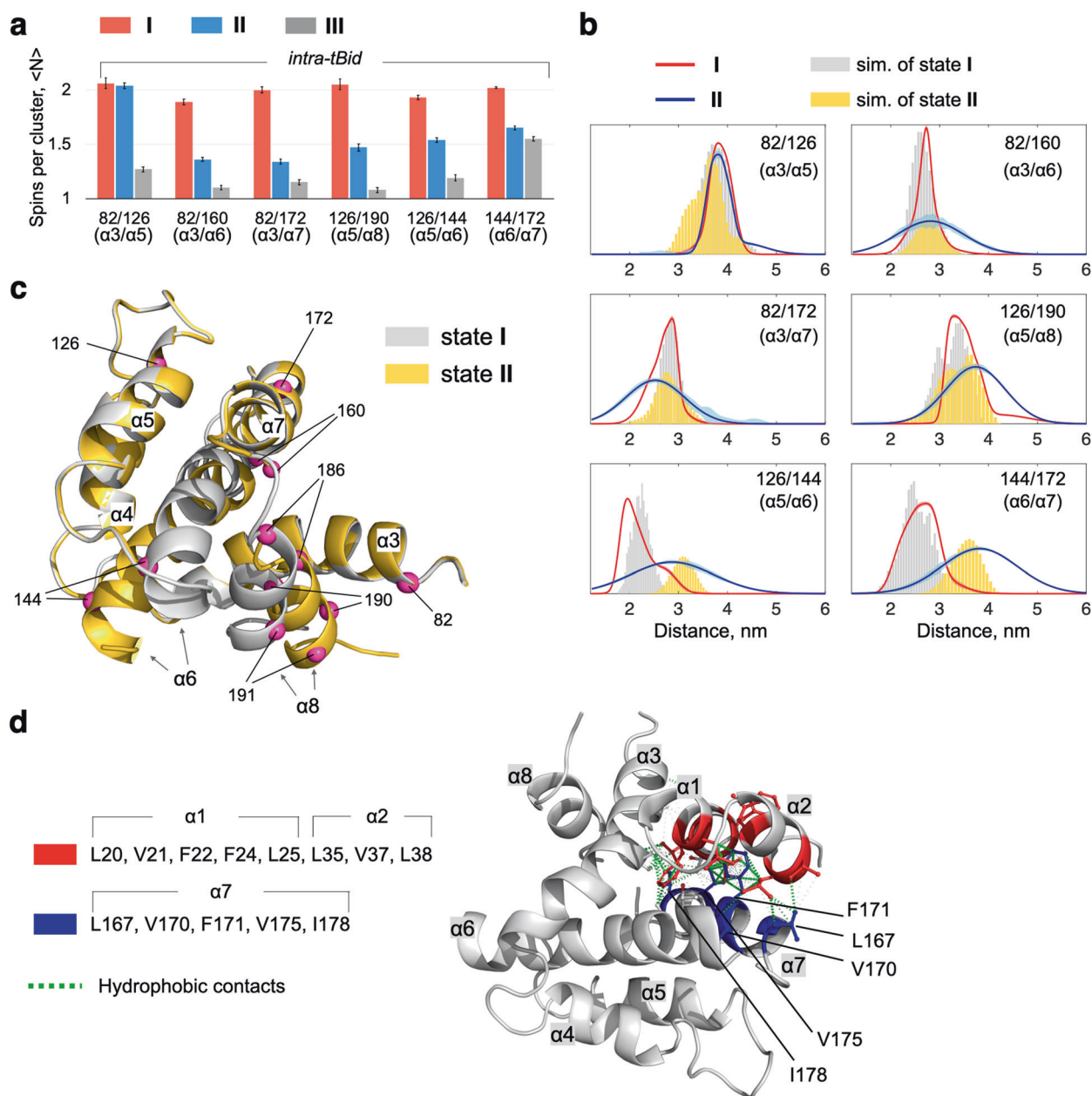
Fig. 3 DEER data of tBid. a The number of spins per cluster calculated from the modulation depth of the DEER data for samples of the intra-tBid group. Error estimates were obtained from the data analysis using the DeerAnalysis. **b** Distance distributions extracted from the DEER data (Supplementary Fig. 5). Distances appear to distribute broadly in the mitochondria-bound state **II**. Predictions simulated from the structure of state **I** and the proposed model of state **II** are reasonably consistent with the DEER results. Shaded bands are estimates of uncertainty in the DEER distance distributions. **c** Cartoon models highlighting the conformational differences of tBid between states **I** and **II**. The major rearrangements occur in helices α6 and α8. **d** Strong hydrophobic interactions occur at the interface between the p7 (α1-α2) and α7 of tBid in the cBid structure of state **II**.

The tBid fragment adopts multiple extended conformations at mitochondria

To identify the conformational changes of tBid (which has more biological significance than p7), we performed DEER measurements (Fig. 3) on samples of the intra-tBid group. The analysis (Fig. 3a) of the modulation depths yielded

<N> values showing that except for 82/126, <N> largely decreased upon the association with mitochondria. (The exception case will be discussed in the next paragraph.) As spin labels were attached to tBid rather than the leaving fragment p7, the reduction in <N> suggested that tBid structure is extended with a great disorder such that the number of specifically interacting spin pairs is decreased.

Our DEER results showed that the distance distributions of double-labeled tBid (Fig. 3b) are clearly different (except 82/126) between states **I** and **II**, partially consistent with the previous results [42]. The distance distributions of state **I** are compatible with the predictions simulated from the NMR-based structure of state **I**. Results of state **II** displayed a much broader distance distribution than state **I**, suggesting that tBid adopts some conformational changes, characterized by extended and relatively disordered structural features, to stay in the membrane-associated state **II**. It suggests that the major changes between **I** and **II** occur in helices α6–α8. It is thus reasonable to observe that the distance distribution of 82/126 (α3/α5) changes little between **I** and **II**. Also, we observed that while the 82/126 (α3/α5) distance distribution remains largely the same, the distance distributions of 82/160 (α3/α6) and 126/144 (α5/α6) widen in state **II**. As α6 sits between α3 and α5 in the hydrophobic core of cBid, one would predict (as demonstrated in a later section) that the increased flexibility in α6 is related to the association with mitochondrial membranes. We also measured interspin distances of the samples in state **III** (Supplementary Fig. 5), but most of the data were characterized by small modulation depths and thus their distance distributions could not be reliably extracted.

Based on the distance distributions, we modeled the conformation of cBid in **II** (Fig. 3c) and simulated distance distributions (yellow histograms in Fig. 3b) from the derived model using the MtsslWizard. The simulations are consistent with the dominant peaks of the DEER distance distributions, and thus are considered to be a representative of the conformations. The DEER distance distributions are clearly greater in distribution width than the simulations, suggesting a large variation in the ensemble of tBid conformations in state **II**. The structure of tBid in state **II** is more disordered and flexible as compared to that in state **I**.

p7 and tBid remain held together in state II, primarily by hydrophobic interactions

Together, our DEER results (Figs. 2 and 3) indicate that the p7 fragment remain in contact with tBid until the presence of BAX that promotes the transition from **II** to **III**. To provide more support for this finding, we performed calculations using the protein interaction calculator (PIC) [43] and the Arpeggio program [44] to evaluate the hydrophobic interactions at the p7/tBid interface (Fig. 3d). This analysis relied on the hydrophobic interaction defined in the Arpeggio program to extract nearest-neighbor atoms within a 0.5 nm radial cutoff. We carried out the calculation for residues 16–38 of the p7 fragment in the modeled cBid structure of state **II**, as these residues are at the p7/tBid interface. We found that there are 129 inter-atomic hydrophobic contacts

(green dashed line) at the interface, which totally contribute about 30 kcal/mol to stabilizing the p7/tBid complex. Particularly, the apolar residues L167, V170, F171, V175 and I178 (blue) form a large hydrophobic surface and face toward the apolar residues of the p7 fragment (red). These calculations suggest that the p7 and tBid fragments are held tightly together via hydrophobic interactions in state **II**.

PEGylation studies reveal changes in the local environment of individual helices

Next, we performed PEGylation gel shift assays on single-cysteine variants of cBid to investigate the change in the local environment of individual helices during the activation. Briefly, cBid mutants were incubated in a desired state for 30 min, followed by a 1 h incubation at room temperatures with/without cysteine-reactive 2 kDa PEG-maleimide. The gel shift profiles were visualized by running on SDS-PAGE, followed by immunoblotting (IB) to obtain quantitative descriptions for PEG-labeling efficiency (see Methods). To demonstrate this approach, we carried out the experiments on two solvent-exposed sites (128 and 188) and one buried site (134) of cBid in state **I**. The solvent-exposed sites were clearly shifted in the results (Fig. 4a), confirming the feasibility of the PEGylation assay to study the local environment of cBid. A site with PEG-labeling efficiency less than half of the maximum obtained (~37% as indicated by yellow dashed line in Fig. 4a) is considered to be a buried or less buried site in this study. Specifically, we categorized the data into four groups: solvent exposed (>47%), less exposed (37–47%), less buried (27–37%), and buried (<27%). The PEG-labeling efficiency increases with increasing local solvent accessibility.

BH3 domain of α3 is exposed to solvent upon the association with mitochondria

We performed the PEGylation assays to explore the change in the local environment of α3 (Fig. 4b). In state **I**, site 82 was clearly solvent-exposed as compared to other three sites (87, 91, and 97), consistent with the expectation for the structure of state **I** (Fig. 4c). In state **II**, all of the four sites were found to become solvent-exposed, revealing a drastic change in the local solvent accessibility of α3. In state **III**, the four sites retained a similar (or less) solvent accessibility as state **II**. Our results provided quantitative descriptions for the local changes and thus revealed (Fig. 4c) molecular details about the local environment of α3. We found that α3, which comprises the important BH3 domain (as denoted in Fig. 1a), is buried within cBid structure in state **I**, whereas it becomes largely exposed to solvent in both **II** and **III**. The BH3 domain is exposed and free to interact with either
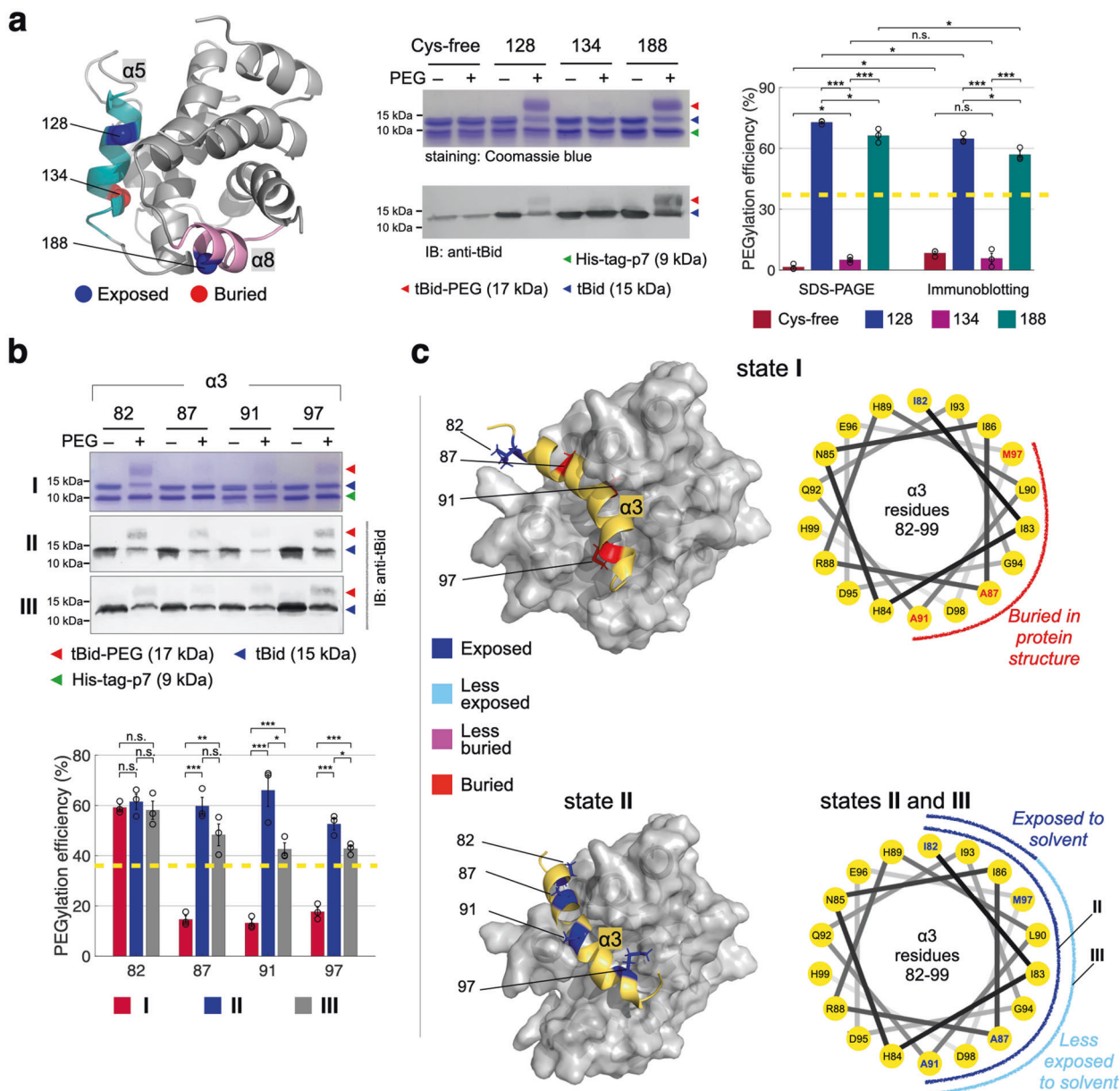
Fig. 4 PEG-labeling study of α3. a Locations of sites 128, 134, and 188 in Bid (state **I**). The PEGylation-based gel shift assays allow us to evaluate the local environment of individual sites by the PEG-labeling efficiency. Concentration of cBid was 10 μM. PEG-labeling efficiency greater (or less) than 37% is considered to indicate a solvent-exposed (or buried) environment in the present study. **b** Results of the PEGylation assay and the PEG-labeling efficiency for α3. Drastic changes in the local environment of 87, 91, and 97 were observed between **I** and **II**. Error bars represent the mean ± SE from three independent experiments. **c** Cartoon models illustrating the changes in the local environment of α3.

pro-survival or multi-BH-domain pro-apoptotic proteins in states **II** and **III**.

Drastic changes in α6–α8 occur during the membrane associations

We also performed the PEGylation assays to explore changes in the local environments of α6–α8 (Fig. 5a). For α6, site 144 was highly exposed in state **I**, but it became

clearly buried in states **II** and **III**. Other two sites 156 and 160 of α6 were observed to remain in a relatively buried environment, with minor variations over the three states. As our DEER results supported that tBid adopts an extended conformation in state **III**, we can thus reasonably attribute the low PEG-labeling efficiency of these sites in **III** to the association with mitochondrial membranes.

As for α7, sites 167, 169, and 172 behaved similarly over the three states: they were highly solvent-exposed in **I**,
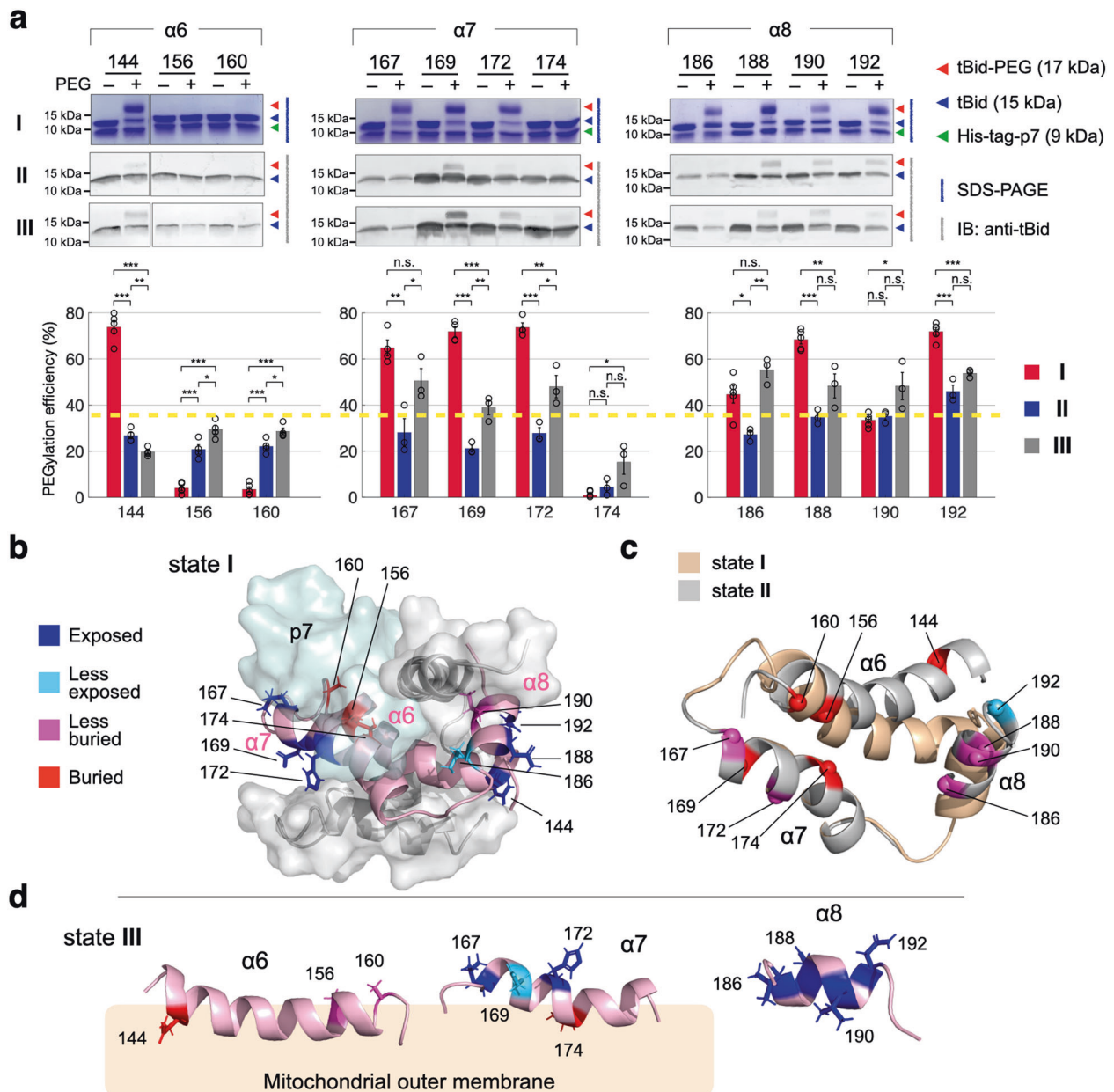
Fig. 5 PEG-labeling study of α6–α8. a Results of the PEGylation assay and the PEG-labeling efficiency for helices α6–α8. Error bars represent the mean ± SE from at least three independent experiments. **b** A cartoon model showing the studied sites in cBid state **I**. Structures of p7 and α3–α5 are shown in surface representation to highlight the location of α6–α8. **c** Cartoon models showing the structural differences of α6–α8 between states **I** and **II**. Except for site 192, all of the studied sites in state **II** were in a buried or less buried environment, as suggested from the PEGylation results. **d** Profiles of local PEG-labeling efficiency for α6–α8 in state **III**. The local solvent accessibility in (**c** and **d**) is colored according to (**b**).

clearly buried in **II**, and reverted to being exposed (or less exposed) in **III**. On the contrary, site 174 (α7) remained buried over the three states. As for α8, four sites 186, 188, 190, and 192 were studied. The first three sites were observed to behave similarly over the states: they were less buried in **II** and exposed (or less exposed) in **I** and **III**. Site 192 (α8) remained solvent-exposed over the states.

These quantitative data allowed us to reveal the local changes of α6–α8. The local solvent accessibility in state **I**

are well consistent with the expectation from the state **I** structure (Fig. 5b). In state **II** (Fig. 5c), all of the studied sites except 192 were buried, experiencing a distinct reduction in the solvent accessibility as opposed to state **I**. The reduction is likely caused by the association with mitochondrial membranes in state **II** that promotes the burial of the residues in the membranes. In state **III** (Fig. 5d), tBid adopts a highly extended conformation at mitochondrial membrane. Although the extended
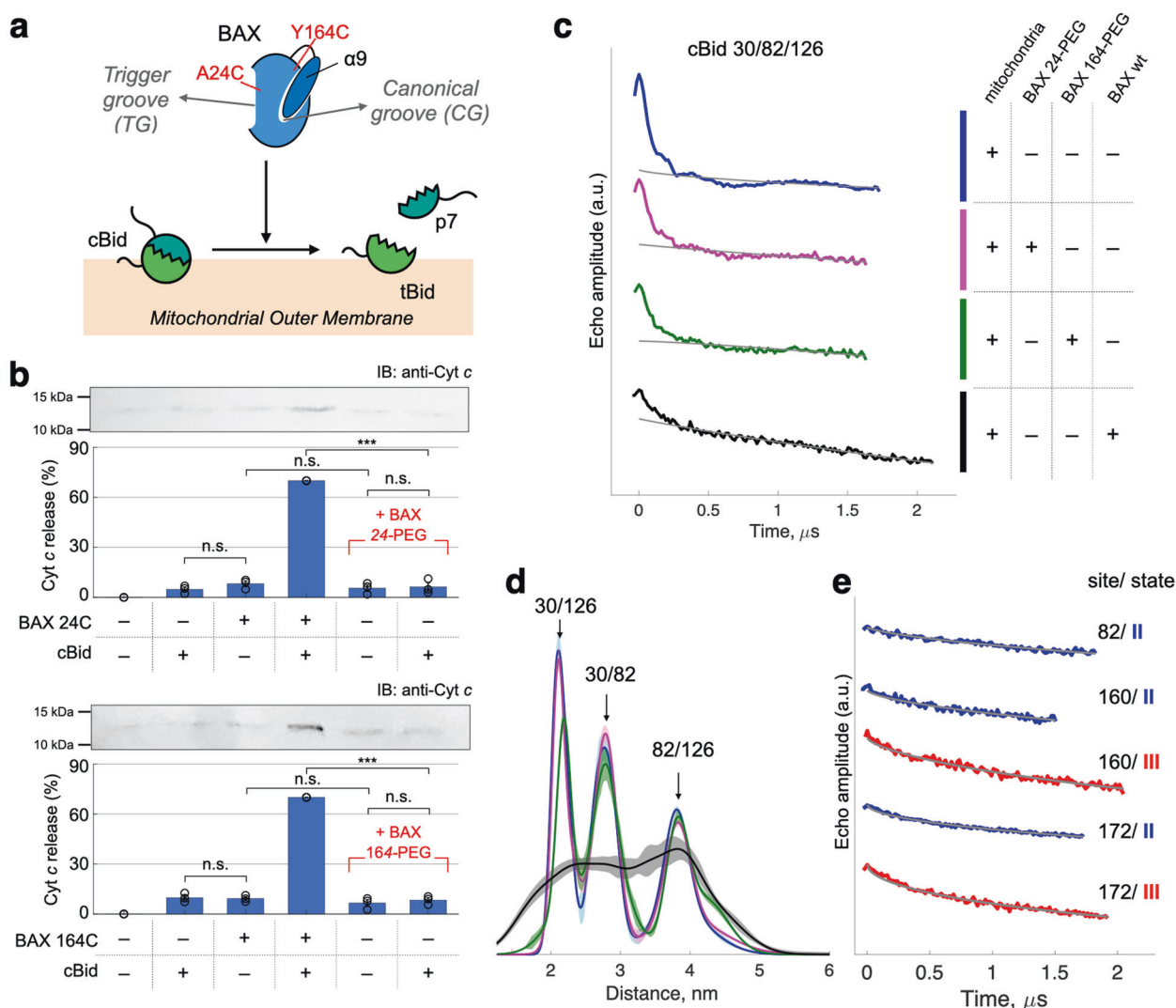
Fig. 6 Interaction between cBid and BAX. a Cartoon illustration of the binding grooves in BAX and the cBid/BAX interaction. **b** Evaluation of the ability of BAX mutants (with/without PEG-labeling) to induce cytochrome *c* release from mitochondria. Grooves TG and CG of BAX are important in associating with cBid at mitochondria. Error bars represent the mean ± SE from three independent experiments. **c** Time-domain DEER data of triple-labeled cBid 30/82/126. A large reduction in the modulation depth of DEER signals, which indicates the breakup of cBid, was only observed in the presence of BAX wt.

d Distance distributions of the triple-labeled cBid. They are colored according to (**c**). Shaded bands are estimates of uncertainty in the DEER distance distributions. **e** Time-domain DEER data of single-labeled cBid. They show primarily exponential decay (gray lines), suggesting a homogeneous dispersion of cBid at mitochondria. The decay of the data changes little with states, indicating no sign of networked aggregations of cBid in real mitochondria. See also Supplementary Fig. 6.

conformation of tBid was not determined here, the local environments of individual helices in state **III** were revealed in this study. A large portion of helices α7 and α8 became solvent-exposed in state **III**.

Membrane-associated cBid interacts with BAX and Mtch2 to induce MOMP

Our results presented above support a view (Fig. 6a) that cBid associates with BAX at mitochondrial membranes and the association is critical to cause the large structural

changes of tBid, leading to the dissociation of p7 from cBid. Below, we performed more experiments to validate the suggested molecular association.

Previous reports have identified two distinct grooves in BAX that regulate BAX activation by BH3-derived peptides or cBid. The two key grooves are (Fig. 6a) the C-terminal canonical binding groove (CG; also known as the canonical BH3 binding groove) comprising α2-α5, and the distinct TG located between α1 and α6 of BAX [11, 21–23]. It was demonstrated that when either of the grooves is blocked by site-directed PEGylation from interacting with activators,

BAX remains inactive and loses the ability to cause MOMP [21]. Following the experimental strategy [21], we prepared two single-cysteine variants of BAX, A24C and Y164C, which are located in TG and CG grooves, respectively, and performed cytochrome c release assays. Our results (Fig. 6b) confirmed that when either of the grooves is shielded by PEG-labeling, BAX cannot be activated by cBid to cause MOMP. (Supplementary Fig. 2b shows more supporting results performed with the BAX$^{-/-}$BAK$^{-/-}$ DKO cells.)

Next, we investigated how the conformation of cBid is changed in response to different BAX, including wt, 24-PEG, and 164-PEG. We performed DEER measurements on a triply spin-labeled cBid (30/82/126) in the presence of mitochondria together with different BAX variants. The DEER traces (Fig. 6c) of the triple-labeled cBid with either BAX 24-PEG or 164-PEG displayed high similarity to that obtained in the absence of BAX, all of which are characterized by distinct dipolar signals and high amplitudes of modulation depth. It was only when BAX wt was used that we observed a clear decrease in the modulation depth of the DEER trace (black trace in Fig. 6c). The decrease indicates the separation of p7 from tBid and the formation of an extended conformation of tBid at mitochondrial membrane.

The corresponding distance distributions (Fig. 6d) support our observations above. Distance distributions obtained without BAX and with PEGylated BAX (24-PEG or 164-PEG) are similar to each other, featured by three distinct distance peaks corresponding to the three interspin pairs in cBid 30/82/126. When BAX wt was added that would interact with cBid and induce MOMP, the resultant distances appeared broadly distributed, supporting an extended conformation of tBid at mitochondria in state **III**. Besides, this study also investigated whether the reported cBid model for state **II** is related to a state cBid bound to Mtch2 in mitochondria. Using the mitochondria isolated from Mtch2$^{-/-}$ knockout HCT116 cells, our results (Supplementary Fig. 6) showed that Mtch2 plays a role in the reported cBid model in state **II**, and that the presence of Mtch2 (together with BAX) is also critical to promoting the extended conformation of tBid in state **III**. Together, our results support that the interactions among cBid, BAX, and Mtch2 in mitochondrial membranes seem imperative and might be the driving force for the conformational transition of cBid from states **II** to **III**.

No sign of tBid aggregates on mitochondria in state III

We also performed DEER measurements on singly spin-labeled cBid to investigate whether tBid proteins form a networked aggregate (or oligomer) on mitochondria. If cBid proteins form a specific pattern of assembly, we expect to see a noticeable increase in the modulation depth (caused by intermolecular distances among the aggregates of single-labeled cBid) and a site-dependent change in the slope of DEER signals (due to different interspin distances in the aggregate that affect local spin concentrations). Our DEER data (Fig. 6e) showed that the signals are dominated by a similar background decay regardless of the incubated state (**II** or **III**) and spin-labeling site. We thus concluded that the cBid samples are being homogeneously dispersed on the membrane and they do not form any specific patterns of aggregate at mitochondrial membranes.

Discussion

Conformation of cBid in real mitochondria is unclear from previous studies

It has been generally accepted that the tBid fragment can induce BAX activation in a lipid environment that leads to membrane pores [45]. As such, plenty of studies have only focused on exploring the conformation of tBid in lipid membranes. Using fluorescence techniques, tBid was reported to undergo multiple structural rearrangements into a superficially membrane-bound state on mitochondria-like membrane vesicles or supported lipid bilayers [42, 46]. Oh et al. studied tBid conformations in vesicles resembling the lipid composition of the mitochondrial outer membrane contact sites and reported that tBid is partially unfolded with only one side of α6–α8 buried in the lipid bilayers at shallow depths, without spanning the bilayer [47]. NMR studies of the purified tBid fragment showed that tBid in detergent micelles adopts an extended configuration rather than a compact fold and that its BH3-containing α3 is associated with the micelles, suggesting an "on the membrane" binding mode for tBid interaction with BAX [20]. Using live-cell quantitative FRET-imaging, Gahl et al. showed that the p7 fragment is free to diffuse away after caspase-8 cleavage and that tBid and BAX can form a self-propagating network at the initiation of staurosporin-induced apoptosis [19]. An emerging picture consistent with these previous results is that p7 is separated from tBid after the initial binding of cBid to the membrane (or detergents) and then tBid acquires an extended conformation pivotal for promoting intermolecular contacts with BAX. However, molecular details about how the individual helices of cBid (i.e., the p7/tBid complex) interact with real mitochondrial membranes as well as BAX during the activation process are unclear from these previous studies.

The inactive-to-active transition of cBid occurs at mitochondrial membranes

This study has investigated the conformational changes of cBid during its association with BAX at real mitochondrial membranes that leads to BAX-mediated MOMP. Mitochondria used in this study were isolated from either mouse liver or the $BAX^{-/-}BAK^{-/-}$ DKO HCT116 cells. We provide new perspectives regarding the Bid activation by dividing the process into three distinct states and investigating the activation in a stepwise manner.

Cleaved Bid was found to retain a compact structure highly similar to its native, un-cleaved structures (Supplementary Fig. 1) [40]. Upon association with mitochondrial membranes, cBid adopts an altered conformation, readily accessible for the engagement with pro-apoptotic BAX protein. Our results reveal that the cBid conformation in this membrane-associated state (i.e., state **II**) is characterized by major helical rearrangement in helices α6–α8, which renders the three helices largely buried, and a sharp increase in the solvent accessibility of BH3-containing α3, while the structural integrity of cBid is basically preserved. The exposure of the BH3 domain is believed to be critical to the subsequent BAX/BAK activation. An improved picture of the mitochondria-associated cBid is thus uncovered in the present study.

After incubating the membrane-bound cBid with BAX (state **III**), we found that the p7 fragment is largely separated from the membrane-bound complex and the tBid fragment is induced by the association with BAX to develop an ensemble of highly extended conformations. The extended conformation of tBid is consistent with the previous results obtained in the mitochondrial-like vesicles or detergent micelles [19, 20, 42]. However, our results support that the extended conformation of tBid results from the association with BAX, Mtch2, and mitochondrial membrane, rather than with membrane alone. Moreover, we show no sign of formation of tBid aggregates on real mitochondrial membranes.

In conclusion, we reveal molecular details of the Bid activation at real mitochondrial membranes in a stepwise manner. The association of cBid with membranes and Mtch2 initiates structural rearrangements that unmask the BH3 domain, priming it for engagement with BAX to induce BAX-mediated MOMP. It is the interactions among cBid, BAX, and Mtch2 at mitochondrial membranes that further trigger the fragmentation of cBid and drive the conformation of tBid from a compact ensemble to an ensemble of highly extended conformations. However, the activated tBid fragments do not assemble into an aggregate in mitochondrial membranes. This study provides a better understanding of the cBid-induced BAX activation and the refined model might lead to an effective treatment that can specifically target different functional states of Bid to suppress the cBid-induced BAX activation.

Materials and methods

Recombinant protein preparation

Bid expression and purification

Full-length mouse Bid was cloned into *NdeI/XhoI* site of pET28a vector (New England Biolabs, Inc.). Wild-type (wt) Bid has two native cysteine residues (C30 and C126). Cysteine-free construct (C30S/C126S) was used to prepare single- or multiple-cysteine variants of Bid mutant for spin-labeling and PEGylation studies. Point mutations of recombinant Bid were generated using the QuikChange site-directed mutagenesis kit (Stratagene) and verified by DNA sequencing. The recombinant pET28a vector was transformed into the E. coli BL21(DE3) expression strain (Novagen). Recombinant proteins fused with six histidines at the N-terminal of Bid were expressed and purified by an affinity Ni-column, as previously described [48]. Briefly, bacterial culture was grown at 37 °C in Luria−Bertani (LB) medium containing kanamycin (30 μg/mL) until OD600 reached 0.6–0.8. Protein expression was induced by addition of 1 mM IPTG (isopropyl 1-thio-β-D-galactopyranoside) at 30 °C for 4–6 h. The cell pellet was collected by centrifugation and resuspended in ice-cold lysis buffer (20 mM Tris, pH 7.4, 100 mM NaCl, 20 mM imidazole and protease inhibitor tablet (cOmplete)). The resuspended pellet was sonicated on ice for 5 min, followed by centrifugation at 13000 *g* for 40 min. The supernatant was filtrated through a 0.22 μm filter and then loaded onto an affinity Ni column using HisTrap HP (GE Healthcare) at a flow rate about 1 mL/min. The column was washed with 10 column volumes (CV) of wash buffer (50 mM Tris, pH 7.4, 500 mM NaCl and 40 mM imidazole). Bid fraction was eluted with 10 CV of elution buffer-1 (20 mM Tris, pH 7.4, 100 mM NaCl and 100 mM imidazole) and elution buffer-2 (20 mM Tris, pH 7.4, 100 mM NaCl and 500 mM imidazole). Purified protein was confirmed by sodium dodecyl sulfate-polyacrylamide gel electrophoresis (SDS-PAGE) with Coomassie blue staining. Imidazole was removed using a PD-10 desalting column (GE Healthcare) equilibrated with storage buffer (20 mM Tris, pH 7.4, and 100 mM NaCl), and protein concentration was estimated via absorption spectroscopy at 280 nm.

Caspase-8 expression and purification

The truncated human caspase-8 (ΔDEDs-Casp-8, amino acids 217–496) was cloned into NdeI/BamHI site of

pET15b vector (New England Biolabs, Inc.), as previously reported [48]. The recombinant pET15b vector was transformed into the E. coli BL21(DE3) pLysS expression strain (Novagen). Recombinant proteins fused with six histidines at the N-terminal of caspase-8 were expressed and purified by an affinity Ni-column followed by size exclusion chromatography (SEC). Bacterial culture was grown at 37 °C in 2xYT medium containing 100 μg/mL ampicillin (Amp) until OD600 reached 0.6–0.8. Protein expression was induced by addition of 0.2 mM of IPTG at 37 °C for 4–6 h. Cells were harvested by centrifugation and resuspended in ice-cold lysis buffer (50 mM Tris, pH 7.4, 100 mM NaCl, 20 mM imidazole, and 1 mM PMSF). The resuspended pellet was sonicated on ice for 5 min, followed by centrifugation at 13000 g for 40 min. The supernatant was filtrated through a 0.22 μm filter and then loaded onto an affinity Ni-column using HisTrap HP (GE Healthcare) at a flow rate about 1 mL/ min. Unbound proteins were removed with 10 CV of wash buffer (50 mM Tris, pH 7.4, 500 mM NaCl and 40 mM imidazole). Caspase-8 fraction was eluted with elution buffer (50 mM Tris, pH 7.4, 100 mM NaCl and 500 mM imidazole). Protein was then further purified with storage buffer (20 mM Tris, pH 7.4, and 100 mM NaCl) by SEC using a HiLoad 16/60 Superdex 75 column (GE Healthcare). The purified caspase-8 was confirmed by SDS-PAGE with Coomassie blue staining. Protein concentration was estimated via absorption spectroscopy at 280 nm.

BAX expression and purification

Full-length BAX and mutants were prepared as previously described [17]. Mouse BAX was cloned into pTYB1 vector (New England Biolabs, Inc.), resulting pTYB1-BAX construct. The pTYB1-BAX construct encoding a fusion protein of BAX with chitin binding peptide was separated by a self-cleavable intein tag to obtain a full-length BAX. Wild-type (wt) BAX has two native cysteine residues at 62 and 126. Cysteine-free construct (C62S/C126S) was used to prepare single-cysteine variants of BAX, A24C and Y164C. Point mutations of recombinant BAX were generated using a QuikChange mutagenesis kit and verified by DNA sequencing. Proteins were expressed in E. coli (ER2566) strain (New England Biolabs, Inc.) and purified without detergent. Bacterial cultures were grown at 37 °C in LB medium containing 0.1 g/L Amp to reach an OD600 of 1.0. Protein expression was induced by addition of 0.3 mM IPTG at 30 °C for 6–8 h. The cells were harvested by centrifugation and resuspended in ice-cold lysis buffer (20 mM Tris-HCl, pH 7.4, 500 mM NaCl, and 1 mM PMSF). The resuspended pellet was sonicated on ice for 30 min, followed by centrifugation at 13000 g for 50 min. The soluble fraction was loaded onto chitin affinity resin column at the flow rate about 0.5 mL/min, and unbound proteins were washed with lysis buffer. The resin was incubated in a equilibrated buffer (20 mM sodium phosphate, pH 8.0, 100 mM NaCl, and 60 mM dithiothreitol (DTT)) for 48 h. Proteins were eluted from column and further purified by a SEC using a HiLoad 16/60 Superdex 75 column (GE Healthcare) in PB buffer (20 mM sodium phosphate, pH 7.4, 100 mM NaCl). Purified proteins were confirmed by SDS-PAGE with Coomassie blue staining. Protein concentration was determined using absorption spectroscopy at 280 nm.

To generate PEGylated BAX, purified BAX mutants A24C and Y164C were incubated in the presence of five-fold excess of 2 kDa Poly(ethylene glycol) methyl ether maleimide (mPEG-mal) in PB buffer overnight at room temperature. To remove residual mPEG-mal and unmodified BAX mutants, 5 mL HiTrap Q HP anion exchange chromatography column (Q-column) (GE Healthcare) was used. Sample was loaded onto Q-column pre-equilibrated in 20 mM Tris (pH 7.4) and eluted by an NaCl step gradient with an elution buffer (20 mM Tris, pH 7.4, 1 M NaCl). Flow rate for binding and elution was set to 5 mL/min. PEGylated BAX mutants were confirmed by SDS-PAGE with Coomassie blue staining.

Activation of BAX by cBid

BAX monomer was incubated in PB buffer (20 mM sodium phosphate, pH 7.4, 100 mM NaCl), with cBid in PB buffer, and with cBid in PB buffer containing 0.5% mild detergent CHAPS at room T for 12 h. The concentrations of BAX and cBid are both 25 μM during incubations. The final incubated volume was adjusted to 500 μL. The oligomerization of BAX were then verified by SEC using a HiLoad 16/60 Superdex 75 column (GE Healthcare) with PB buffer. The chromatogram (Supplementary Fig. 1b) demonstrated monomeric fractions at 80 mL and oligomeric fractions approximately within 50 ml. The molecular weight of the oligomer is ~440 kDa, consistent with the previous studies [21, 24].

Mitochondria isolation and cytochrome c release assays

Mouse liver tissue (0.2 mg) was ground using a douce homogenizer with 15–20 strokes, and the mitochondria were separated using centrifugation according to Mitochondria Isolation Kit (Thermo Scientific). The mitochondria were then washed with Mitochondria Assay Buffer A (MAB A: 200 mM mannitol, 68 mM sucrose, 10 mM HEPES-KOH pH 7.4, 110 mM KCl, 1 mM EDTA, 1 mM EGTA, 0.1% bovine serum albumin, protease inhibitor) and centrifuged at 12000 g, and the supernatant was removed. The pellet was resuspended using enough MAB B (i.e.,

MAB A without 0.1% BSA) and then quantified by Bradford assay (Bio-Rad) to yield a final protein content of mitochondrial fraction was 3 mg/mL. The final mitochondria fraction was placed on ice for further downstream processing or stored at $-80\,°C$ with additional 300 mM trehalose for future use [49]. For the cytochrome c release assay, 10 µL of mitochondria fraction (100 µg of protein) were incubated with recombinant cBid (20 nM), BAX or PEGylated BAX mutants (100 nM) at $37\,°C$ for 30 min. cBid was prepared by simultaneously incubating full-length Bid (20 nM), caspase-8 (20 nM) and DTT (1 mM) in the mitochondria solution. The final volume was adjusted to 30 µL. The sample was then centrifuged at 12000 g for 5 min separating the supernatant and pellet fractions. The supernatant was subjected to subsequent IB. Quantification of immunoblots was done using ImageJ software (version 1.49, NIH). The fraction of cytochrome c released (%) is calculated by $(I-I_0)/(I_{max}-I_0) \times 100\%$, where I_{max} and I_0 are the analyzed intensities of cytochrome c obtained in the presence and absence of activated BAX.

It is noteworthy that the results of the present study are primarily based on the use of cBid, BAX, and mitochondria, all of which are from mouse. Experiments with mitochondria isolated from the $BAX^{-/-}BAK^{-/-}$ DKO HCT116 cells were also performed to ensure that the presence of trace amounts of BAX and BAK in mouse mitochondrial outer membranes makes no difference to the trend observed in the results with mouse mitochondria.

Cell culture and mitochondria isolation from $BAX^{-/-}BAK^{-/-}$ double knockout HCT116 cells and $Mtch2^{-/-}$ knockout HCT116 cells

$BAX^{-/-}BAK^{-/-}$ double knockout (DKO) HCT116 cells were kindly given by Dr. R. Youle [50] (NIH, Bethesda, MD). Cells were cultured in 5% CO_2 at $37\,°C$ and grown in McCoy's 5A medium supplemented with 4 mM L-glutamine, 1 mM non-essential amino acids, 10% heat-inactivated FBS, 100 U/mL penicillin and 100 mg/mL streptomycin. Mitochondria from DKO cells were isolated using the method previously described [51]. Approximately 90% confluent cells from five 75 cm^2 flasks were washed once with phosphate-buffered saline (PBS), detached by trypsinization and gentle pipetting, and spun down in a table centrifuge at room temperature (1500 g, 5 min). The pellet was washed twice with cold PBS and resuspended in mitochondrial isolation buffer (MIB: 200 mM D-mannitol, 68 mM sucrose, 10 mM HEPES, pH 7.4, 10 mM KCl, 1 mM EDTA, 1 mM EGTA, 0.1% BSA, protease inhibitor). The cell suspension was incubated on ice for 15 min and homogenized using a 2 mL dounce homogenizer with 50 strokes. The homogenate was centrifuged at 1000 g for 10 min at $4\,°C$, and the supernatant was collected and

centrifuged again using the same conditions to ensure that no unlysed cells or nuclei were present. The resulting supernatant was centrifuged at 8000 g at for 10 min at $4\,°C$. The pellet was collected as the heavy membrane (i.e., mitochondrial) fraction. The mitochondrial fraction was resuspended using enough MIB (~100 µL) to yield final OD600 of 6. Following the previously established protocol [17], we measured the release of cytochrome c caused by BAX A24C and Y164C with and without the PEGylation treatment. The results with the mitochondria of DKO cells (Supplementary Fig. 2b) are consistent with the results with mitochondria of mouse livers presented in Fig. 6.

$Mtch2^{-/-}$ knockout (KO) HCT116 cells were kindly given by Dr. David C. S. Huang (WEHI, Australia) [52]. $Mtch2^{-/-}$ KO cells were cultured in 5% CO_2 at $37\,°C$ and grown in RPMI1640 medium supplemented with L-glutamine, 10% FBS, 100 U/mL penicillin and 100 mg/mL streptomycin. Mitochondria from $Mtch2^{-/-}$ KO cells were isolated following the same protocol used for the isolation of mitochondria from the $BAX^{-/-}BAK^{-/-}$ DKO cells. The mitochondrial fraction was resuspended using enough MIB (ca. 100 µL) to yield final OD600 of 6. The mitochondrial suspension (200 µL MIB with OD600 of 6) were centrifuged and collected as heavy membrane (mitochondrial) fraction for further study.

Immunoblotting

Samples were resolved by 15% SDS-PAGE and electroblotted onto a 0.45 µm PVDF membrane (GE Healthcare). Primary antibodies used were anti-mouse Bid cleavage (59/60) site (Millipore) and mouse anti-cytochrome c antibodies (clone 7H8.2C12, Millipore). Detection was achieved using donkey anti-rabbit IgG HRP (GE Healthcare) and sheep anti-mouse IgG HRP (GE Healthcare) secondary antibodies. Proteins were visualized by 4CN Plus Chromogenic Substrate (PerkinElmer). Quantification of partition of tBid was performed using the ImageJ software (version 1.49, NIH).

PEGylation-based gel shift assay

For PEGylation assays of cBid in states **II** or **III**, purified single-cysteine variants of cBid mutant (15 µM) were incubated with isolated mouse mitochondria fraction (100 µg of proteins) in the absence (state **II**) or presence (state **III**) of BAX wt (7.5 µM) at $37\,°C$ for 30 min. The final volume was adjusted to 30 µL. After incubation, the sample was centrifuged at 17000 g for 10 min to pellet the mitochondria fraction. The pellet fraction was separated from supernatant and washed by ice-cold TBS buffer to remove peripherally attached cBid, followed by an extra centrifugation procedure at 17000 g for 10 min to obtained cBid-bound pellet fraction. The pellet fractions were then

resuspended with 10 μL TBS buffer (20 mM Tris, pH 7.0, 100 mM NaCl) and reacted with or without 2 kDa mPEG-mal (500 μM) in TBS buffer at room temperature for 1 h. For PEGylation assays of cBid in state **I**, purified cBid proteins (10 μM) in TBS buffer were reacted with or without tenfold excess of 2 kDa mPEG-mal (100 μM) at room temperatures for 1 h. The reaction volume was adjusted to 20 μL. After reaction, the samples were quenched with DTT (25 mM) and solubilized in 1% (w/v) SDS. The samples were electrophoresed on SDS-PAGE (for state **I**) and immunoblotted (for states **II** and **III**) with anti-mouse Bid cleavage (59/60) site antibody, which specifically recognizes tBid fragment.

To calculate the cysteine accessibility to 2 kDa mPEG-mal, the fractions of tBid (blue triangles in Figs. 4, 5) in SDS-PAGE or IB were quantified using ImageJ software. The PEGylation efficiency (%) is calculated by $(I_0–I)/I_0 \times 100\%$, where I and I_0 are the band intensities (blue triangles in Figs. 4, 5) with and without the reaction of mPEG-mal, respectively. The bands of tBid-PEG (red triangles) were not used in the analysis because the conjugation of PEG affects the recognition of antibody.

Continuous wave (cw)-ESR spectroscopy and preparation of spin-labeled cBid

To generate cBid, purified cysteine variants of Bid proteins (1 mg/mL) were incubated with recombinant caspase-8 (25 μg/mL) in the presence of 10 mM DTT for more than 16 h at room temperatures. The cleavage efficiency was checked by SDS-PAGE with Coomassie blue staining, and DTT was removed using a PD-10 desalting column equilibrated with storage buffer. Purified cBid proteins were then labeled with a tenfold excess of (1-oxy-2,2,5,5-tetramethyl-3-pyrroline-3-methyl) methanethiosulfonate spin label (MTSSL) (Alexis Biochemicals, San Diego, CA) per cysteine residue overnight in the dark at 4 °C. PD-10 desalting column pre-equilibrated with storage buffer was used to remove free MTSSL.

To prepare samples in state **I**, spin-labeled variants of cBid were concentrated by centrifugation, followed by the addition of glycerol to yield ~40 μL solution volume (containing 30% (v/v) glycerol as a cryoprotectant). To prepare cBid samples in states **II** and **III**, isolated mitochondria fraction (2500 μg of proteins) from mouse liver was incubated with spin-labeled cBid (400 μg) in the absence (state **II**) or presence (state **III**) of BAX wt in a molar ratio of cBid:BAX 2:1 at 37 °C for 30 min. The final volume of the incubated mixture was adjusted to 133 μL by storage buffer. After incubation, the sample was centrifuged at 17000 g for 30 min to pellet the mitochondria fraction. The pellet fraction was separated from supernatant and then resuspended by ice-cooled storage buffer (>1 mL) to remove peripherally

attached cBid proteins on mitochondrial membranes, followed by an extra centrifugation procedure at 17000 g for 30 min to collect the mitochondrial pellet fraction. Finally, glycerol was added to yield a solution volume of 30 μL (containing 20% (v/v) glycerol as a cryoprotectant) in a quartz ESR tube. The final concentration of cBid was ~0.3 mM. A Bruker ELEXSYS E580 cw/pulsed spectrometer was used. Cw-ESR experiment was performed at an operating frequency of 9.4 GHz with incident microwave power 1.5 mW. Each spectrum was recorded with a magnetic width of 150G, 1024 points, and 20–40 scans at 300K.

DEER distance measurements and molecular modeling

For DEER experiments, d8-glycerol were used as cryoprotectant for the preparation of cBid samples. All buffers in the DEER experiments were deuterated. The concentration of cBid in the DEER measurements was ~0.3 mM. The samples were loaded into the quartz ESR tube (i.d. 3 mm) and plunge-cooled in liquid nitrogen before DEER measurement. A Bruker ELEXSYS E580-400 pulsed spectrometer, with a split-ring resonator (EN4118X-MS3) and a helium gas flow system (4118CF and 4112HV), was used. ESR probe head (ER4118X-MS3) was precooled to 80 K using a helium flow system prior to the transfer of the ESR sample tube into the cavity. DEER experiments were carried out by using the typical four-pulse constant-time DEER sequence as previously described [17, 24, 25]. The detection pulses were set to 32 and 16 ns for π and π/2 pulses, respectively, and the pump frequency was set to ~70 MHz lower than the detection pulse frequency. The pulse amplitudes were chosen to optimize the refocused echo. The π/2-pulse was employed with +x/−x phase cycles to eliminate receiver offsets. The duration of the pumping pulse was about 32 ns, and its frequency was coupled into the microwave bridge by a commercially available setup (E580-400U) from Bruker. All pulses were amplified via a pulsed traveling wave tube amplifier (E580-1030). The field was adjusted such that the pump pulse is applied to the maximum of the nitroxide-based MTSSL spectrum. The accumulation time for each set of data was about 12 h at a temperature of 80 K.

The determination of interspin distance distribution of the DEER spectroscopy was performed using time-domain analysis by Tikhonov regularization based on the L-curve method, followed by a data refinement process using the maximum entropy method (MEM) to obtain non-negative distance distributions [37, 38]. The recovered distance distributions were checked against modeled distances for spin-label rotamers attached to protein structures. The modeled distances were obtained using the program MtsslWizard [41], which operates as a plugin of the PyMol. MtsslWizard searches for ensembles of possible MTSSL rotamers that do

not clash with a static model of the protein. This program has been evaluated in a number of challenging studies and demonstrated that it is useful to predict experimental data rather well. The benefits of the program are its accuracy and simplicity. There are 20 NMR models for full-length Bid structure (PDB: 1DDB). All structural models of cBid in this study started from models 13 because it was determined to be one of the most representative models using the Olderado program [53]. To model the conformations of cBid in states **I** and **II**, we assumed that (1) the helical segments are rigid, (2) and the linker regions are flexible.

Calculation of the number of spins per cluster from DEER data

The modulation depth (V_m) of time-domain DEER data can be analyzed to estimate the number of coupled spins <N> in cBid using the previously developed method [36]. <N> is calculated by $<N> = 1 + \ln(1 − V_m)/\ln(1 − \lambda)$, where λ is a scalar value representing the fraction of the spins (in the sensitive distance range of DEER, ~6 nm in the present study) that is excited by the pump pulse. Sample cBid 144/160, whose <N> is close to 2 over the three states, was used as a reference to evaluate λ values of other samples. For cBid mutants in state **I**, averages of λ values are ~0.29 (triply labeled cBid) and 0.30 (doubly labeled cBid). In states **II** and **III**, λ values are slightly affected due to the complexity of lipid environment and thus reduced to ~0.20 (**II**) and 0.22 (**III**). One fast and convenient way to obtain the information of the modulation depth and background function is to analyze the raw DEER experimental data using the DeerAnalysis software package [39].

Statistics and reproducibility

The statistical analyses were based on a one-way ANOVA test ($^{n.s.}p > 0.05$; $*p \leq 0.05$; $**p \leq 0.01$; $***p \leq 0.001$). The exact p values are indicated either directly in the figure or in the legend. The exact sample size is given in the legend of each figure. The mean ± standard error (SE) is displayed, unless otherwise stated. The standard deviation is not displayed if it is smaller than the corresponding symbol.

Author contributions CLH and YWC designed the experiments and analyzed the data. CLH, HHC, and SWL performed all the experiments. CLH and YWC wrote the paper. All authors discussed the results and commented on the paper.

Compliance with ethical standards

Conflict of interest The authors declare that they have no conflict of interest.

Publisher's note Springer Nature remains neutral with regard to jurisdictional claims in published maps and institutional affiliations.

References

1. Youle RJ, Strasser A. The BCL-2 protein family: opposing activities that mediate cell death. Nat Rev Mol Cell Biol. 2008; 9:47–59.
2. Czabotar PE, Lessene G, Strasser A, Adams JM. Control of apoptosis by the BCL-2 protein family: implications for physiology and therapy. Nat Rev Mol Cell Biol. 2014;15:49–63.
3. Tait SWG, Green DR. Mitochondria and cell death: outer membrane permeabilization and beyond. Nat Rev Mol Cell Biol. 2010;11:621–32.
4. Li H, Zhu H, Xu CJ, Yuan J. Cleavage of BID by caspase 8 mediates the mitochondrial damage in the Fas pathway of apoptosis. Cell. 1998;94:491–501.
5. Kantari C, Walczak H. Caspase-8 and Bid: caught in the act between death receptors and mitochondria. Biochim Biophys Acta - Mol Cell Res. 2011;1813:558–63.
6. Shamas-Din A, Brahmbhatt H, Leber B, Andrews DW. BH3-only proteins: orchestrators of apoptosis. Biochim Biophys Acta - Mol Cell Res. 2011;1813:508–20.
7. Leber B, Geng F, Kale J, Andrews DW. Drugs targeting Bcl-2 family members as an emerging strategy in cancer. Expert Rev Mol Med. 2010;12:e28.
8. Hinds MG, Smits C, Fredericks-Short R, Risk JM, Bailey M, Huang DCS, et al. Bim, Bad and Bmf: intrinsically unstructured BH3-only proteins that undergo a localized conformational change upon binding to prosurvival Bcl-2 targets. Cell Death Differ. 2007;14:128–36.
9. Chou JJ, Li H, Salvesen GS, Yuan J, Wagner G. Solution Structure of BID, an Intracellular Amplifier of Apoptotic Signaling. Cell. 1999;96:615–24.
10. Petros AM, Olejniczak ET, Fesik SW. Structural biology of the Bcl-2 family of proteins. Biochim Biophys Acta. 2004;1644:83–94.
11. Suzuki M, Youle RJ, Tjandra N. Structure of Bax: coregulation of dimer formation and intracellular localization. Cell. 2000;103:645–54.
12. Kuwana T, Mackey MR, Perkins G, Ellisman MH, Latterich M, Schneiter R, et al. Bid, Bax, and Lipids Cooperate to Form Supramolecular Openings in the Outer Mitochondrial Membrane. Cell. 2002;111:331–42.
13. Yethon JA, Epand RF, Leber B, Epand RM, Andrews DW. Interaction with a membrane surface triggers a reversible conformational change in Bax normally associated with induction of apoptosis. J Biol Chem. 2003;278:48935–41.
14. Huang K, Zhang J, O'Neill KL, Gurumurthy CB, Quadros RM, Tu Y, et al. Cleavage by caspase 8 and mitochondrial membrane association activate the BH3-only protein bid during TRAIL-induced apoptosis. J Biol Chem. 2016;291:11843–51.
15. Westphal D, Dewson G, Menard M, Frederick P, Iyer S, Bartolo R, et al. Apoptotic pore formation is associated with in-plane insertion of Bak or Bax central helices into the mitochondrial outer membrane. Proc Natl Acad Sci USA. 2014;111:E4076–85.
16. Moldoveanu T, Grace CR, Llambi F, Nourse A, Fitzgerald P, Gehring K, et al. BID-induced structural changes in BAK promote apoptosis. Nat Struct Mol Biol. 2013;20:589–97.
17. Lai Y-C, Li C-C, Sung T-C, Chang C-W, Lan Y-J, Chiang Y-W. The role of cardiolipin in promoting the membrane pore-forming

activity of BAX oligomers. Biochim Biophys Acta - Biomembr. 2019;1861:268–80.

18. Li MX, Tan IKL, Ma SB, Hockings C, Kratina T, Dengler MA, et al. BAK α6 permits activation by BH3-only proteins and homooligomerization via the canonical hydrophobic groove. Proc Natl Acad Sci. 2017;114:7629–34.

19. Gahl RF, Dwivedi P, Tjandra N. Bcl-2 proteins bid and bax form a network to permeabilize the mitochondria at the onset of apoptosis. Cell Death Dis. 2016;7:e2424.

20. Wang Y, Tjandra N. Structural insights of tBid, the caspase-8-activated bid, and its BH3domain. J Biol Chem. 2013;288:35840–51.

21. Lan Y-J, Wang Y-T, Hung C-L, Chiang Y-W. PEGylation-based strategy to identify pathways involved in the activation of apoptotic BAX protein. Biochim Biophys Acta - Gen Subj. 2020;1864:129541.

22. Czabotar PE, Westphal D, Dewson G, Ma S, Hockings C, Fairlie WD, et al. Bax Crystal Structures Reveal How BH3 Domains Activate Bax and Nucleate Its Oligomerization to Induce Apoptosis. Cell. 2013;152:519–31.

23. Gavathiotis E, Suzuki M, Davis ML, Pitter K, Bird GH, Katz SG, et al. BAX activation is initiated at a novel interaction site. Nature. 2008;455:1076–81.

24. Sung T-C, Li C-Y, Lai Y-C, Hung C-L, Shih O, Yeh Y-Q, et al. Solution Structure of Apoptotic BAX Oligomer: Oligomerization Likely Precedes Membrane Insertion. Structure. 2015;23:1878–88.

25. Jeschke G. DEER Distance Measurements on Proteins. Annu Rev Phys Chem. 2012;63:419–46.

26. Lai Y, Kuo Y, Chiang Y. Identifying Protein Conformational Dynamics Using Spin-label ESR. Chem – Asian J. 2019;14:3981–91.

27. Georgieva ER, Borbat PP, Ginter C, Freed JH, Boudker O. Conformational ensemble of the sodium-coupled aspartate transporter. Nat Struct Mol Biol. 2013;20:215–21.

28. Martens C, Stein RA, Masureel M, Roth A, Mishra S, Dawaliby R, et al. Lipids modulate the conformational dynamics of a secondary multidrug transporter. Nat Struct Mol Biol. 2016;23:744–51.

29. Raemy E, Montessuit S, Pierredon S, van Kampen AH, Vaz FM, Martinou J-C. Cardiolipin or MTCH2 can serve as tBID receptors during apoptosis. Cell Death Differ. 2016;23:1165–74.

30. Katz C, Zaltsman-Amir Y, Mostizky Y, Kollet N, Gross A, Friedler A. Molecular Basis of the Interaction between Proapoptotic Truncated BID (tBID) Protein and Mitochondrial Carrier Homologue 2 (MTCH2) Protein. J Biol Chem. 2012;287:15016–23.

31. Zaltsman Y, Shachnai L, Yivgi-Ohana N, Schwarz M, Maryanovich M, Houtkooper RH, et al. MTCH2/MIMP is a major facilitator of tBID recruitment to mitochondria. Nat Cell Biol. 2010;12:553–62.

32. Kurokawa T, Okamura Y. Mapping of sites facing aqueous environment of voltage-gated proton channel at resting state: A study with PEGylation protection. Biochim Biophys Acta - Biomembr. 2014;1838:382–7.

33. Robin AY, Iyer S, Birkinshaw RW, Sandow J, Wardak A, Luo CS, et al. Ensemble Properties of Bax Determine Its Function. Structure. 2018;26:1346. e5

34. McDonald SK, Levitz TS, Valiyaveetil FI. A Shared Mechanism for the Folding of Voltage-Gated K + Channels. Biochemistry. 2019;58:1660–71.

35. Borbat PP, Freed JH. Pulse Dipolar Electron Spin Resonance: Distance Measurements. In: Timmel C, Harmer J, editors. Structural Information from Spin-Labels and Intrinsic Paramagnetic Centres in the Biosciences. Structure and Bonding, vol 152. Berlin, Heidelberg: Springer; 2013, p. 1–82.

36. Bode BE, Margraf D, Plackmeyer J, Durner G, Prisner TF, Schiemann O. Counting the monomers in nanometer-sized oligomers by pulsed electron - Electron double resonance. J Am Chem Soc. 2007;129:6736–45.

37. Chiang Y-W, Borbat PP, Freed JH. The determination of pair distance distributions by pulsed ESR using Tikhonov regularization. J Magn Reson. 2005;172:279–95.

38. Chiang Y-W, Borbat PP, Freed JH. Maximum entropy: a complement to Tikhonov regularization for determination of pair distance distributions by pulsed ESR. J Magn Reson. 2005;177:184–96.

39. Jeschke G, Chechik V, Ionita P, Godt A, Zimmermann H, Banham J, et al. DeerAnalysis2006—a comprehensive software package for analyzing pulsed ELDOR data. Appl Magn Reson. 2006;30:473–98.

40. McDonnell JM, Fushman D, Milliman CL, Korsmeyer SJ, Cowburn D. Solution Structure of the Proapoptotic Molecule BID: a Structural Basis for Apoptotic Agonists and Antagonists. Cell. 1999;96:625–34.

41. Hagelueken G, Abdullin D, Schiemann O. mtsslSuite: Probing biomolecular conformation by spin-labeling studies. Methods Enzymol. 2015;563:595–622.

42. Shamas-Din A, Bindner S, Zhu W, Zaltsman Y, Campbell C, Gross A, et al. tBid undergoes multiple conformational changes at the membrane required for bax activation. J Biol Chem. 2013;288:22111–27.

43. Tina KG, Bhadra R, Srinivasan N. PIC: protein Interactions Calculator. Nucleic Acids Res. 2007;35:W473–6.

44. Jubb HC, Higueruelo AP, Ochoa-Montaño B, Pitt WR, Ascher DB, Blundell TL. Arpeggio: a Web Server for Calculating and Visualising Interatomic Interactions in Protein Structures. J Mol Biol. 2017;429:365–71.

45. Billen LP, Shamas-Din A, Andrews DW. Bid: a Bax-like BH3 protein. Oncogene. 2008;27:S93–104.

46. Shivakumar S, Kurylowicz M, Hirmiz N, Manan Y, Friaa O, Shamas-Din A, et al. The proapoptotic protein tbid forms both superficially bound and membrane-inserted oligomers. Biophys J. 2014;106:2085–95.

47. Oh KJ, Barbuto S, Meyer N, Kim R-S, Collier RJ, Korsmeyer SJ. Conformational changes in BID, a pro-apoptotic BCL-2 family member, upon membrane binding. A site-directed spin labeling study. J Biol Chem. 2005;280:753–67.

48. Hung C-L, Lin Y-Y, Chang H-H, Chiang Y-W. Accessing local structural disruption of Bid protein during thermal denaturation by absorption-mode ESR spectroscopy. RSC Adv. 2018;8:34656–69.

49. Yamaguchi R, Andreyev A, Murphy AN, Perkins GA, Ellisman MH, Newmeyer DD. Mitochondria frozen with trehalose retain a number of biological functions and preserve outer membrane integrity. Cell Death Differ. 2007;14:616–24.

50. Wang C, Youle RJ. Predominant requirement of Bax for apoptosis in HCT116 cells is determined by Mcl-1's inhibitory effect on Bak. Oncogene. 2012;31:3177–89.

51. Renault TT, Floros KV, Chipuk JE. BAK/BAX activation and cytochrome c release assays using isolated mitochondria. Methods. 2013;61:146–55.

52. Djajawi TM, Liu L, Gong J, Huang AS, Luo M, Xu Z, et al. MARCH5 requires MTCH2 to coordinate proteasomal turnover of the MCL1:NOXA complex. Cell Death Differ. 2020;27:2484–99.

53. Kelley LA, Gardner SP, Sutcliffe MJ. An automated approach for defining core atoms and domains in an ensemble of NMR-derived protein structures. Protein Eng Des Sel. 1997;10:737–41.